Evaluation of reptation-based modeling of entangled polymeric fluids including chain rotation via nonequilibrium molecular dynamics simulation

Mohammad Hadi Nafar Sefiddashti, Brian J. Edwards,* and Bamin Khomami†
Materials Research and Innovation Laboratory, Department of Chemical and Biomolecular Engineering, University of Tennessee, Knoxville, Tennessee 37996, USA
(Received 16 May 2017; published 9 August 2017)

Recent simulation results of a moderately entangled linear polyethylene $C_{700}H_{1402}$ liquid have confirmed prior simulation and experimental evidence that individual polymer molecules experience periodic rotation and retraction cycles under steady shear flow at high Weissenberg number. With this insight, theoreticians have begun to grapple with this additional complicating physical phenomenon that needs to be incorporated into rheological models to help explain the data under conditions of high shear. In this paper we examine these recent efforts by using nonequilibrium molecular dynamics simulations to provide insight into the requisite theoretical variables and their assigned evolution equations to evaluate the capability of these tube-based models to predict accurately the simulated data sets. This analysis reveals that the primary variables used in tube models to impart a conceptual basis to the theory, namely, the tube orientation tensor and the tube stretch, remain fundamental system properties even far away from equilibrium; however, the theory describing their evolution under flow is not well suited to quantitative prediction. Furthermore, it is demonstrated that key system properties, such as the entanglement number and disengagement time, should play a more significant role in model development since these quantities can change dramatically under flow, particularly at high Weissenberg number where the chain rotation and retraction cycles dominate the system physics.

DOI: 10.1103/PhysRevFluids.2.083301

I. INTRODUCTION

Four and a half decades have passed since de Gennes [1] formulated the basic tenets of reptation theory to describe the dynamics and structure of polymeric fluids, conceptualized by the key idea that each polymer molecule was constrained to move within a tube formed by entanglements between its immediate neighbors. Several years later, Doi and Edwards [2] extended this reptation-based theory in an attempt to explain the dynamics of polymeric liquids under flow. Despite the successful predictions of the theory at low deformation rates, it failed at capturing flow properties within the nonlinear viscoelastic regime, even for the simplest case of monodisperse linear polymers [3]. The most noted problem with the Doi-Edwards (DE) model was the decreasing trend of shear stress in the nonlinear viscoelastic flow regime in the case of steady shearing flows. This resulted in the appearance of a maximum in steady-state shear stress at shear rates $\dot{\gamma}$ around τ_d^{-1}, where τ_d is the disengagement or reptation time of the macromolecules; however, the subsequent negative slope of the shear stress profile has not been observed experimentally.

Marrucci and Grizzuti [4] introduced the concept of chain stretch and employed it to formulate a refinement of reptation theory (the DEMG model). This model improved the DE model by allowing the primitive path of the chain, which was held fixed in the DE model, to increase from its equilibrium

*Corresponding author: bje@utk.edu
†Corresponding author: bkhomami@utk.edu

value for shear rates beginning around τ_R^{-1}, where τ_R is the Rouse relaxation time of the chains. Although the DEMG model was successful at qualitatively predicting the overshoots in shear stress and first normal stress difference after startup of fast shearing flows, at steady state it was only qualitatively reasonable at deformation rates higher than τ_R^{-1} and did not alleviate the decreasing trend of steady-state shear stress within the shear rate range $\tau_d^{-1} < \dot{\gamma} < \tau_R^{-1}$, which is known as the plateau region [5].

Mead *et al.* [5] believed that convective constraint release (CCR), which was initially proposed by Marrucci [6], was the key to understanding the decreasing trend of the shear stress within the plateau region. The dynamical effects of CCR were incorporated into the DE equations by several groups [5,7–11], improving the reptation model predictions significantly within the shear-rate range of $\tau_d^{-1} < \dot{\gamma} < \tau_R^{-1}$. Despite this achievement, the model predictions still diverged from experiments at high deformation rates. To note one specific discrepancy between theory and experiment to be discussed below, the observed experimental overshoot and subsequent undershoot of the transient shear viscosity at high shear rates cannot yet be understood using reptation-based models [12].

Recent atomistic simulations of unentangled and moderately entangled linear polyethylene melts [13–18] demonstrated that individual chain molecules experience retraction and rotation cycles at moderate to high shear rates with a characteristic time scale that scales as $\dot{\gamma}^{\alpha}$, where $\alpha \approx -0.8$ for mildly and moderately entangled liquids [14,15]. The chain rotation is induced by the flow vorticity once the entanglement network within the liquid is partially destroyed by the orienting and stretching of the individual chains comprising the confining tubes. These simulations revealed that individual chain rotation is an important relaxation mechanism over a wide range of shear rates, beginning roughly at $\dot{\gamma} \approx \tau_R^{-1}$, and is the dominant mechanism at high shear rates. This conclusion suggests that this previously unobserved dynamical phenomenon might possibly help to explain the inability of tube-based reptation models to capture the rheological behavior observed in experiments at high shear rates.

Based upon this concept, Costanzo *et al.* [12] proposed that the discrepancy between their recent experimental results and reptation-based theory predictions at high shear rates was possibly due to the absence of a chain-tumbling mechanism in the aforementioned models. Reasoning that the chain rotation and retraction cycles of the individual chains affected the magnitude of the average degree of tube stretch, they introduced a tumbling function into the model evolution equations and compared the resulting predictions with their experiments. They demonstrated that this modification improved the model performance for transient shear viscosity at high shear rates. Specifically, their model predictions for transient shear viscosity at high shear rates exhibited an initial overshoot followed by an undershoot that matched fairly well with their experimental data. Hence, they concluded that chain tumbling could possibly explain the physical origin of the stress undershoot, which had heretofore not been observed in reptation-based theory.

Recently, Stephanou *et al.* [19] rediscovered a model originally proposed by Curtiss and Bird [20], which they aptly dubbed the "tumbling-snake" model, and supplemented it with a nonconstant link tension coefficient. A key component of this model, previously overlooked, was a nonvanishing rotational Brownian contribution that accounted for chain tumbling. This model successfully predicted the undershoot in transient viscosity of entangled polystyrene solutions at high shear rate provided that the additional rotational contribution was included in the model equation set. In the case of entangled polystyrene melts of similar entanglement number, however, no experimental undershoot in transient viscosity was observed, which suggests that the additional rotational contribution might be unnecessary in the case of polymer melts.

In this article we evaluate the model proposed by Costanzo *et al.* [12] using nonequilibrium molecular dynamics (NEMD) simulation results for a moderately entangled polyethylene melt, which are data derived from the massive simulations of our previous work [15]. In particular, we examine the transient viscosity data after startup of shear flow, observing both an overshoot and an undershoot of the viscosity vs time at high shear rate. Concurrently, we also examine the shear behavior of several variations of reptation theory mentioned above in order to draw a better picture of the relevant physics over the entire range of $\dot{\gamma}$.

II. THEORY

We employed a one-mode version of the constitutive model proposed by Costanzo *et al.* [12] and simplified it further by using the differential approximation of the average orientation tensor of the tube segments $\mathbf{S} \equiv \langle \mathbf{uu} \rangle$, where $\mathbf{u}$ is the tube end-to-end unit vector [21,22]. This constitutive model, the DEMG model including chain rotation (DEMGR), is expressed by the set of equations

$$\hat{\mathbf{S}} + 2\boldsymbol{\kappa} : \mathbf{SS} + \frac{1}{\tau_d}\left(\mathbf{S} - \frac{1}{3}\boldsymbol{\delta}\right) = 0, \tag{1}$$

$$\dot{\lambda} = \lambda\boldsymbol{\kappa} : \mathbf{S}\varphi - \frac{k_s(\lambda - 1)}{\tau_R}, \tag{2}$$

$$\boldsymbol{\sigma} = 3G_N^0 k_s \lambda^2 \mathbf{S}, \tag{3}$$

$$k_s = \frac{\left(3\lambda_{\max}^2 - \lambda^2\right)/\left(\lambda_{\max}^2 - \lambda^2\right)}{\left(3\lambda_{\max}^2 - 1\right)/\left(\lambda_{\max}^2 - 1\right)}, \tag{4}$$

in which $\boldsymbol{\kappa}$ is the transpose of the velocity gradient tensor, $\boldsymbol{\delta}$ is the unit tensor, and λ represents the average tube stretch, which is defined as the average tube length normalized by its equilibrium length. Here τ_d and τ_R are the disengagement and the Rouse times, respectively, $\lambda_{\max}$ is the maximum value of the tube stretch (which can be approximated as the ratio of the tube diameter a and Kuhn length b), and G_N^0 is the plateau modulus. In addition, $\hat{\mathbf{S}}$ is the upper-convected derivative of $\mathbf{S}$, defined in the standard fashion, and $\dot{\lambda}$ denotes the material derivative of λ. The tumbling function φ was introduced into Eq. (2) by Costanzo *et al.* [12] in order to incorporate the physical phenomenon of individual chain rotation into the constitutive model. When $\varphi = 1$, Eqs. (1)–(4) reduce to the DEMG model, discussed earlier. The coefficient k_s quantifies the nonlinearity of the effective spring elasticity as described by the inverse Langevin function using the Padé approximation.

In simple shear flow, Costanzo *et al.* [12] proposed the expression for the tumbling function

$$\varphi(t) = \cos(2\pi\omega t)\exp(-\beta t), \tag{5}$$

where ω quantifies the average tumbling frequency of the macromolecules and $1/\beta$ represents the average decorrelation time of the individual chain's end-to-end vectors:

$$\omega = \frac{\mathrm{Wi}_R^{-0.2}}{8\pi}\dot{\gamma}, \tag{6}$$

$$\beta = \frac{\mathrm{Wi}_R^{-0.2}}{8}\dot{\gamma}. \tag{7}$$

In these equations, $\mathrm{Wi}_R = \dot{\gamma}\tau_R$ is the Rouse Weissenberg number. (Note that this is different from the usual Weissenberg number Wi, which is defined based on the disengagement time, i.e., $\mathrm{Wi} = \dot{\gamma}\tau_d$.) It is interesting to note that the tumbling function (5) possesses exactly the same form as the phenomenological fit to autocorrelation function data obtained via the NEMD simulations of Kim *et al.* [13,16] and Nafar Sefiddashti *et al.* [14,15]. Furthermore, the scalings with respect to shear rate described by Eqs. (6) and (7) are consistent with the NEMD data of Nafar Sefiddashti *et al.* [15] as well.

Given the functional form of Eq. (5), it is evident that the tumbling function vanishes under steady-state shear flow (i.e., $t \to \infty$). A possibly unintended consequence of this fact is that the DEMGR model possesses exactly the same steady-state properties as the original DE model; i.e., when $\varphi = 0$, the solution to Eq. (2) is always $\lambda = 1$, corresponding to no stretching of the tubes as in the original Doi-Edwards model. In order to capture the same steady-state rheological property values as the DEMG model that incorporates tube stretch, the tumbling function of Eq. (5) can be

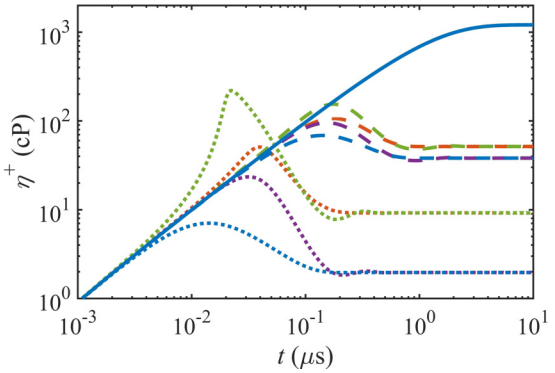

FIG. 1. Predictions of transient shear viscosity at Wi = 0.1 (solid line), Wi = 15 (dashed lines), and Wi = 150 (dotted lines) using the DE (blue), DEMG (red), DEMGR (purple), and DEMGR1 (green) models. The solid blue line represents all models at Wi = 0.1.

replaced by

$$\varphi(t) = \cos(2\pi\omega t)\exp(-\beta t) + 1, \tag{8}$$

in which case $\varphi = 1$ under steady-state conditions. We will refer to this model as DEMGR1.

The liquid examined in this article is a linear $C_{700}H_{1402}$ polyethylene melt at 450 K, which consists of about nine entanglements per chain ($Z = 8.6$) under quiescent conditions. This system has been studied comprehensively in our previous work using NEMD simulations [15]. These prior simulations are the source of the data presented below; however, only Fig. 3 contains previously published data. Based on prior results, $G_N^0 = 1.006$ MPa, $\tau_d = 1216$ ns, $\tau_R = 66$ ns, $a = 42$ Å, and $b = 16.9$ Å [15]. Note that $\lambda_{\max} = \frac{a}{b} \approx 2.5$. We take these values henceforth as the parameters appearing in Eqs. (1)–(8) in order to obtain the predictions of the various constitutive models.

III. RESULTS AND DISCUSSION

Figure 1 displays the transient shear viscosity calculated from the basic DE model, the DEMG model, and the models accounting for tumbling at several values of Wi. This figure shows that the four models collapse onto a single curve at low Wi (equal to 0.1, displayed in the figure as the solid blue line), which is due to the absence of any significant degree of tube stretch and/or chain tumbling at this low flow strength within the linear viscoelastic regime. Note that $\boldsymbol{\kappa} : \mathbf{S} = \dot{\gamma} S_{xy}$ for simple shear flow; hence the first term on the right-hand side of Eq. (2) is very small and therefore $\lambda \approx 1$ at all times.

At higher values of Wi, these models exhibit different transient behavior up to the point where each attains its steady-state value. It is notable that the steady-state values of the DE model and the rotation-enabled DEMGR model are always the same, regardless of Wi; however, there is a gap between these values and the steady-state values of the DEMG and DEMGR1 models, which also are always equivalent. The difference between the two traditional models (i.e., without rotation), the DE and DEMG models, is evidently due to the observation that chain stretch increases with shear rate. Since the DEMGR and DEMGR1 models possess the same steady-state values as the DE and DEMG models, respectively, it is possible that the steady-state value of the shear viscosity can be tuned phenomenologically in a rotation-enabled model simply by replacing the unit value in Eq. (8) with a phenomenologically determined constant α such that $\alpha \sim O(1)$. Nevertheless, the most interesting feature of these data is the noticeable undershoots in the predictions of the rotation-enabled models, which are completely absent in the DE and DEMG models.

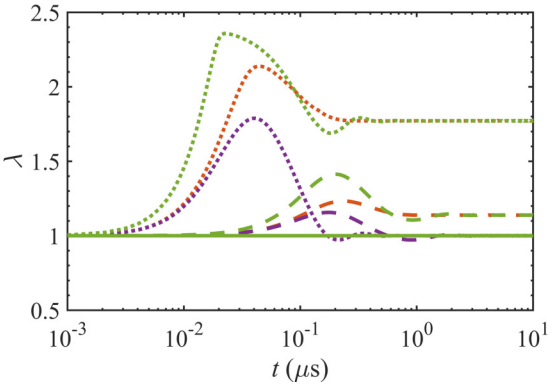

FIG. 2. Chain stretch λ versus time after startup of steady shearing flow. Symbols are as defined in Fig. 1. Note that there are no blue data present because λ is always unity for the DE model at all values of Wi and hence is not plotted. The solid green curve presents all models at Wi = 0.1.

Figure 2 shows the transient behavior of λ arising from the DE, DEMG, and the rotation-enabled models at the same Wi as presented in Fig. 1. In the DE model, there is no mechanism for tube stretch and hence $\lambda = 1$ always; therefore, the data for this model are all included in the solid green line of Fig. 2. At the lowest Wi, λ remains unaltered from the unit value and all models effectively exhibit the DE model behavior. At higher Wi, the DEMG tube stretch increases from the unit value, experiences a maximum, and then eventually settles to a steady-state plateau value that is significantly higher than the DE steady-state unit value, indicating a tube stretch of as much as 50% at Wi = 150. The rotation-enabled models both also exhibit an initial overshoot in the tube stretch, but then reveal a subsequent undershoot before settling down to steady-state plateau values; the DEMGR model attains the same steady-state tube stretch value as the DE model (i.e., $\lambda = 1$), whereas the DEMGR1 model ultimately attains the same steady-state value as the DEMG model at all Wi. This is not surprising given the forms of Eqs. (2), (5), and (8). As $t \to \infty$, Eq. (5) vanishes, as does the first term on the right-hand side of Eq. (2); hence the solution to Eq. (2) is $\lambda = 1$, the same as the DE model. On the other hand, Eq. (8) approaches the unit value as $t \to \infty$, at which time Eq. (2) reduces to the corresponding equation of the DEMG model. Evidently, not only does the steady-state value of the viscosity in Fig. 1 depend critically on the degree of tube stretch, but the transient behavior is also heavily dependent on this parameter, as might have been anticipated from Eq. (3).

It is instructive to examine the steady-state behavior of the viscosity, shear stress, and tube stretch as functions of Wi as obtained from the $C_{700}H_{1402}$ polyethylene liquid simulation described earlier and then to compare them with the available models mentioned above, supplemented by the convective constraint release model of Larson and co-workers [3,5]. This last model is included in this examination because it is widely considered to be the most realistic model within the shear rate range $0 < \dot{\gamma} < \tau_R^{-1}$ since it incorporates both tube stretch and CCR [7–11]; therefore, we will examine this model carefully to see if it can describe the NEMD simulation data any better than the other models.

The Mead-Larson-Doi (MLD) constitutive model is defined by the set of equations [3,5]

$$\frac{1}{\tau} = \frac{1}{\lambda^2 \tau_d} + f(\lambda)\left(\boldsymbol{\kappa} : \mathbf{S} - \frac{\dot{\lambda}}{\lambda}\right), \tag{9}$$

$$\hat{\mathbf{S}}^2 + 2\mathbf{S}^2(\boldsymbol{\kappa} : \mathbf{S}) + \frac{2}{\tau}\mathbf{S} \cdot \left(\mathbf{S} - \frac{1}{3}\boldsymbol{\delta}\right) = 0, \tag{10}$$

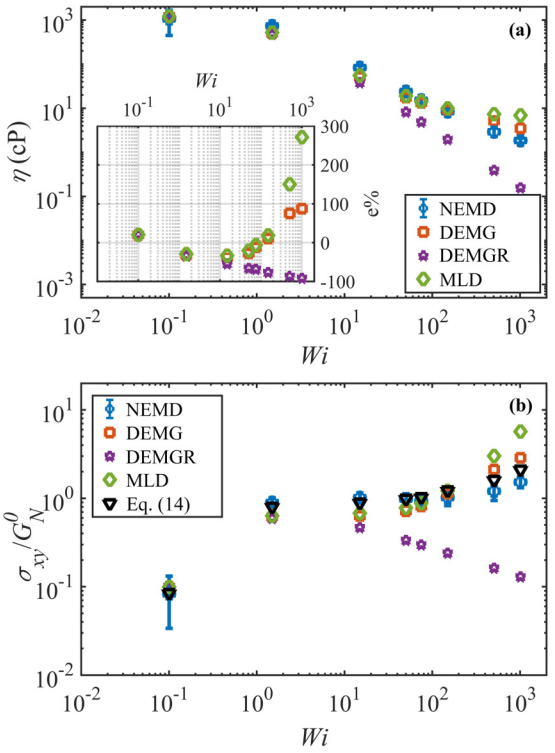

FIG. 3. (a) Steady-state shear viscosity and (b) normalized shear stress from the NEMD simulations (blue circles) plotted alongside predictions of the DEMG (red squares), rotation-enabled DEMGR (purple stars), and MLD (green diamonds) models. The inset in (a) displays the relative error of the various models compared to the NEMD data. The black triangles denote normalized shear stress values calculated using S^t_{xy} via Eq. (14).

$$\dot{\lambda} = \lambda \boldsymbol{\kappa} : \mathbf{S} - \frac{k_s(\lambda - 1)}{\tau_R} - \frac{1}{2}(\lambda - 1)\left(\boldsymbol{\kappa} : \mathbf{S} - \frac{\dot{\lambda}}{\lambda}\right), \tag{11}$$

$$\boldsymbol{\sigma} = 6G_N^0 k_s \lambda^2 \mathbf{S}, \tag{12}$$

where the previously undefined symbol in these equations τ is essentially the disengagement time as corrected according to the CCR effect. In total, these are essentially the equations presented by Mead *et al.* [5], except that the we replaced the original history integral equation for the orientation tensor $\mathbf{S}$ by a differential approximation, which had been initially proposed by Ianniruberto and Marrucci [8]. In addition, $f(\lambda)$ is a switch function that has a value of unity under quiescent conditions but vanishes for highly stretched chains, effectively turning off CCR at high Wi. Herein, we use $f(\lambda) = 1/\lambda$, as suggested by Mead *et al.* [5]. Note that the numerical factor of 6 appearing in the stress expression of Eq. (12) is slightly higher than the factor of 5 introduced by Mead *et al.* [5] in the integral version of the CCR model such that G_N^0 maintains its physical significance as the plateau modulus; however, the factor of 6 is consistent with the analysis of the differential version of the model presented by Marrucci *et al.* [23].

The steady-state viscosity and shear stress (normalized with respect to the plateau modulus) obtained from the NEMD simulations [15] are plotted in Fig. 3 as functions of Wi, along with the solutions for the DEMG, DEMGR, and MLD models. (Keep in mind that the steady-state values for the original DE model are equivalent to those of the DEMGR model and those of the DEMGR1 model

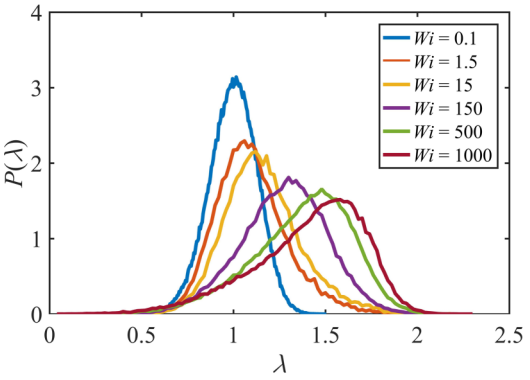

FIG. 4. Probability distribution of the tube stretch variable from the NEMD simulations.

are equivalent to the DEMG model.) As evident from Fig. 3(a), all models exhibit a shear-thinning behavior of the viscosity, but the associated power-law index can vary widely from one model to another, and none of the models matches the NEMD data well at high Wi. The DEMG model, and hence also the DEMGR1 model, comes the closest and thus provides even better predictions for this quantity than the MLD model. Note that by arbitrarily changing the unit digit appearing in Eq. (8) to 0.8, the predictions of the rotation-enabled model can essentially be laid onto the NEMD data (not shown in the figure), although there is no physical rationalization for this occurrence. The shear stress is plotted vs Wi in Fig. 3(b), wherein it becomes evident that the DEMGR model of Costanzo *et al.* [12] is equivalent to the original DE model with regard to the negative slope of shear stress for $\dot{\gamma} > \tau_d^{-1}$; however, the DEMG (and hence DEMGR1) and the MLD models match fairly well the NEMD shear stress throughout the plateau region, but then overpredict the shear stress at high Wi, where the DEMG and DEMGR1 models perform significantly better than the MLD model.

To understand why the model predictions deviate from the NEMD data at high Wi, it is prerequisite to examine the key variables that appear in the model equations, namely, λ and $\mathbf{S}$. The former variable, however, can be problematic to calculate far from quiescent conditions. We illustrate this by plotting the probability distribution function of λ (calculated from the ratio of primitive path length and the ensemble average of the primitive path length under quiescent conditions) at several values of Wi in Fig. 4. At low values of Wi, the distribution is essentially Gaussian, as expected, and the mean and the peak of the distribution hence coincide. However, as Wi increases, the distribution not only shifts to higher values of λ, but also becomes quite broad and skewed to the point where the mean can be significantly lower than the peak position. The effect of this rather unexpected distribution on the calculation of λ is unknown and so in the following we will calculate λ both ways, i.e., in terms of the average (called mean) and the peak position (referred to as mode). Note that in standard tube theory and its refinements, Gaussian statistics are generally assumed, even far from equilibrium.

The steady-state values for the tube stretch as calculated from the NEMD simulations of Nafar Sefiddashti *et al.* [15] are plotted vs Wi in Fig. 5. These data for λ are plotted for both mean and mode, wherein it becomes apparent that the method used to calculate this quantity can change its value dramatically as the distribution of chains broadens in response to the imposed shear field. The discrepancy between the two data sets becomes more pronounced as Wi increases due to the broadening of the chain end-to-end vector distribution in response to the rotational motion of the individual macromolecules (see Fig. 5 of Nafar Sefiddashti *et al.* [15]). The mode form of the tube stretch is always higher than that computed from the mean of the distribution, which is broadly skewed toward smaller λ at higher Wi. Unfortunately, no theoretically definitive method yet exists for determining λ for the non-Gaussian distributions of chain configurations far from equilibrium.

The various model predictions of λ are also presented in Fig. 5. Note that the DE and DEMGR models produce unit values of λ regardless of Wi and therefore these data are not displayed in

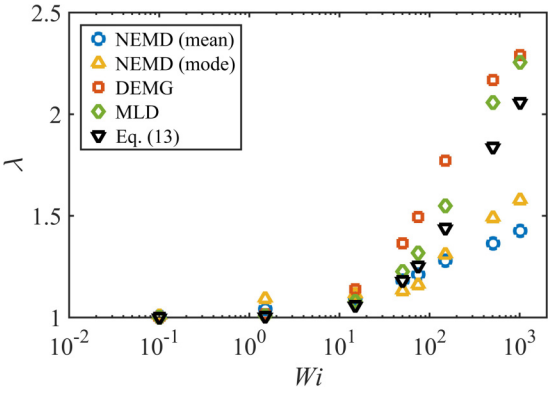

FIG. 5. Tube stretch vs Wi from the NEMD simulations calculated via the mean of the distribution of Fig. 4 (mean value, blue circles) and the peak position (mode value, yellow triangles) plotted alongside predictions of the DEMG (red squares) and MLD (green diamonds) models. Note that the DEMGR1 model λ values are equivalent to the DEMG model steady-state values and that the DE and DEMGR models (not shown) satisfy $\lambda = 1$ at all Wi. The black triangles denote values of λ calculated using S^t_{xy} according to Eq. (13).

the figure. Furthermore, the steady-state values arising from the DEMGR1 model are equivalent to those of the DEMG model. As evident from the figure, there is a very large discrepancy between the model predictions and the NEMD results, with the models vastly overpredicting the simulation data, whether in mean or mode form. Figure 5 shows that λ begins to increase as soon as the flow enters the nonlinear viscoelastic regime, i.e., Wi > 1. Specifically, it increases rapidly with increasing shear rate for $\mathrm{Wi}_R > 1$, which is the region where it is believed that chain stretching becomes an important relaxation mechanism. The chain stretch reaches a rather high value of $\lambda \sim 1.4-1.6$ at very high shear rates, which is roughly 56%–64% of the theoretical value of $\lambda_{\max}$ for this system, demonstrating that chain stretch is not generally negligible in the case of shear flows. Note that there is generally good agreement between the model and NEMD simulation results for Wi < 50; interestingly, this is the Wi at which chain rotation begins to become significant [15]. As previously discussed by Nafar Sefiddashti *et al.* [14], these tumbling events tend to decrease the primitive path length and hence the tube stretch ratio, which suggests that the discrepancy between the model and NEMD data at higher Wi is possibly due to these chain rotation events. This plot also reveals that CCR slightly improves the model performance in predicting λ at steady state for $\dot{\gamma} < \tau_e^{-1}$ as compared to the DEMG and DEMGR1 models, but it does not have a beneficial effect at higher shear rates. This is consistent with previous assertions that CCR is most important within the shear-rate range of $\tau_d^{-1} < \dot{\gamma} < \tau_R^{-1}$ and with the fact that the switch function tends to decrease the effect of CCR at high Wi. In fact, at the highest Wi values examined, the tube stretch as predicted by the models is unrealistically high, presumably being caused by a higher average degree of tube orientation than observed in the NEMD data since the models do not properly incorporate chain rotation and retraction cycles into the chain length distribution function during the averaging. This can be seen more clearly by examining the behavior of $\mathbf{S}$ (specifically, the S_{xy} component), as discussed below in reference to Fig. 6.

The nonzero components of the tube orientation tensor are plotted vs Wi in Fig. 6 (except for S_{zz}, which follows closely the behavior of S_{yy}). The S_{xx} component of the NEMD data and the DEMG and MLD models exhibit the same qualitative behavior, i.e., a slow increase at low Wi, followed by a rapid increase to a plateau value at high Wi. Although the trends are qualitatively consistent, there is a vast quantitative discrepancy between the simulation data and the model predictions over much of the applicable range of Wi, which is particularly egregious for the DEMG model. This model greatly overpredicts the simulation data, suggesting an orientational distribution function that is much narrower and peaked than that of the NEMD data. With regard to S_{yy}, the trend is opposite to that of S_{xx}, showing a decreasing value with increasing Wi. The DEMG model significantly

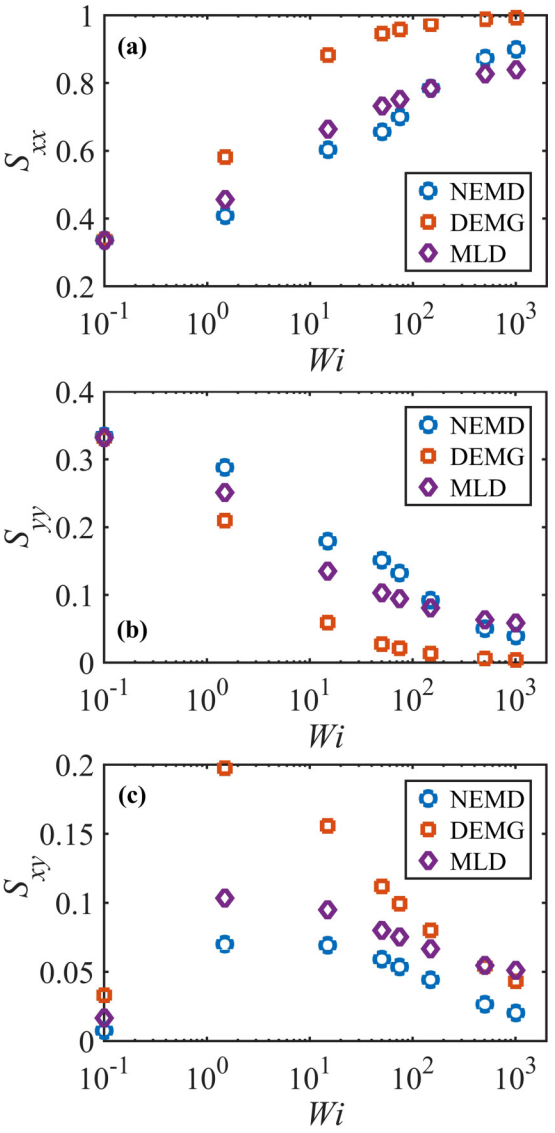

FIG. 6. Nonzero components of the orientation tensor **S** vs Wi from the NEMD simulations (blue circles) plotted alongside predictions of the DEMG (red squares) and MLD (purple diamonds) models. Note that S_{zz} behaves similarly to S_{yy} and is therefore not shown.

underpredicts the NEMD data, which is again indicative of excessive narrowing of the distribution function. The S_{xy} component increases rapidly within the linear viscoelastic regime, obtaining a maximum at Wi ≈ 1, and then experiences a slow decay toward its equilibrium value, indicative of the small orientation angle of the tubes with respect to the flow (x) direction at high Wi. Both the DEMG and MLD models greatly overpredict the NEMD data, once again indicating a much greater degree of alignment than the simulations would suggest.

None of the models discussed above, whether rotation enabled or not, is capable of describing the simulation data over the whole range of Wi with any degree of accuracy. So far, we have traced this problem to inaccurate predictions of the tube stretch and orientation tensor, but the question remains whether this inaccuracy is a fundamental consequence of the choice of the

preaveraged variables (λ and $\mathbf{S}$) or rather is symptomatic of the forms of the various model evolution equations, e.g., Eqs. (1) and (2). In order to examine this issue and possibly attain a minimal level of understanding, we can calculate the quantities λ and $\mathbf{S}$ directly from the NEMD simulation data (as illustrated in Figs. 5 and 6), effectively bypassing the model evolution equations for these variables, and then compare these values directly with those calculated via the various tube models.

As discussed previously, Costanzo *et al.* [12] tried to improve the predictions of the DEMG constitutive model by introducing the individual chain tumbling dynamics into the evolution equation of the tube stretch λ. Here we also focus on tube orientation tensor $\mathbf{S}$ as a major factor in the calculation of stress tensor in tube-based models. Hence we calculate the shear component of the orientation tensor S_{xy} using NEMD simulation results and incorporate it into the tube model in order to calculate the shear stress. The tube orientation tensor, calculated from the NEMD simulation data, is defined as $\mathbf{S}^t = \langle \mathbf{u}^t \mathbf{u}^t \rangle$, where $\mathbf{u}^t$ is the unit end-to-end vector of an entanglement strand. Knowing the number of entanglements Z (as a function of Wi), each chain can be divided into $Z + 1$ segments of an equal number of monomeric units that represent the individual entanglement strands. End-to-end vectors of the entanglement strands can then be easily identified and the appropriate ensemble averages of the components of the orientation tensor are readily calculated from the NEMD data. This allows us to bypass the evolution equation for the tube orientation tensor, such as Eqs. (1) and (10), by inputting directly the corresponding ensemble averages of the components of $\mathbf{S}^t$ into the evolution equation for λ and the expression for the extra stress tensor, such as Eqs. (2) and (3).

Under steady-state conditions, Eq. (2) can be expressed in terms of S^t_{xy} as

$$\lambda \dot{\gamma} S^t_{xy} - \frac{k_s(\lambda - 1)}{\tau_R} = 0, \tag{13}$$

which is obtained from the evolution equation of λ in the DEMG model for a simple shear flow by letting $\dot{\lambda} = 0$; in this way, the evolution equation for $\mathbf{S}$ is bypassed. The black triangles in Fig. 5 denote values of the tube stretch calculated according to Eq. (13). As evident from the plot, values of λ computed in this manner show better agreement with the NEMD values than any of the tube models; however, it remains clear that there still exists a sizable discrepancy between theory and data that must emanate from physical inconsistencies in the tube stretch evolution equation (13).

Similarly, the steady-state shear stress can be calculated using S^t_{xy} according to

$$\sigma_{xy} = 3\bar{G} k_s \lambda^2 S^t_{xy}, \tag{14}$$

which is essentially the Doi-Edwards equation that incorporates the tube-stretching effect, as presented by Eq. (3) of the DEMG model. In Eq. (14), $\bar{G} = 15G^0_N/4$ is an effective elastic modulus that ensures that the definition of the tube orientation tensor used to compute the NEMD simulation data average of this quantity (namely, $\mathbf{S}^t = \langle \mathbf{u}^t \mathbf{u}^t \rangle$) is consistent with the zero-shear viscosity. Alternatively, we could have calculated the plateau modulus according to $G^0_N = \frac{4}{5} \nu k_B T$ and then used Eq. (12) in order to calculate the stress tensor. Either method yields the same features in the rheological properties, as described below. The black triangles in Fig. 3(b) display the data obtained for the normalized shear stress via Eq. (14) as a function of Wi for the $C_{700}H_{1402}$ melt. These data are very close to the shear stress data computed directly from the NEMD simulations, indeed, much closer than any of the tube model variations at high Wi.

Taken together, the results presented above for both tube stretch and shear stress under steady shear support some interesting considerations. As already demonstrated, the values of these two quantities as calculated via Eqs. (13) and (14) reveal the best agreement with the values computed directly from the NEMD simulation data when compared to any of the tube model variations examined herein. Especially noticeable is the improved agreement for Wi $\geqslant$ 150, where the model predictions begin to diverge greatly from the NEMD data. This is the region in which chain tumbling is considered to be the dominant relaxation mechanism of the system [15]. It should also be noted that CCR and chain tumbling are not included explicitly in Eqs. (13) and (14). To be precise, neither equation has the corrections of the MLD model due to CCR [see Eq. (11)] or has the correction of

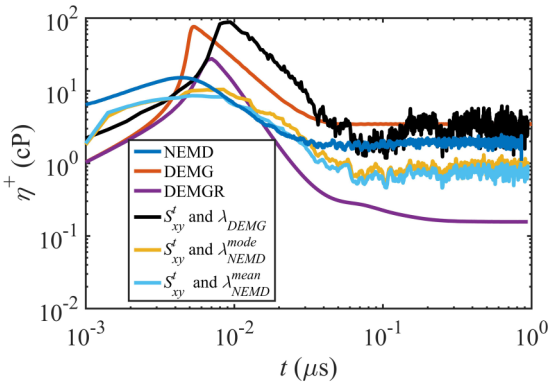

FIG. 7. Transient shear viscosity at Wi = 1000 upon startup of shear flow vs time. The dark blue curve corresponds to data obtained directly from the NEMD simulations. The red and purple curves are the predictions of the DEMG and DEMGR models, respectively. The black curve was obtained using S^t_{xy} computed from the NEMD simulations with λ_{DEMG} calculated via Eq. (2) with $\varphi = 1$ and the shear stress via Eq. (14) and the light blue and yellow curves were obtained using only Eq. (14) with both S^t_{xy} and $\lambda^{\text{mean}}_{\text{NEMD}}$ and both S^t_{xy} and $\lambda^{\text{mode}}_{\text{NEMD}}$, respectively, obtained directly from the simulation data.

the tumbling function φ as proposed in Eq. (2) of the DEMGR model. Instead, the effects of these phenomena are explicitly incorporated into the calculations by using the actual values of S^t_{xy} as obtained directly from the NEMD simulations. The implication is that, at least as far as steady-state shear flow is concerned, both the definitions used to calculate the tube stretch and the orientation tensor are appropriate for this particular case. It also suggests that the tube models employing stress expressions such as Eq. (14) are indeed physically reasonable and capable of quantifying the stress adequately, provided that they can predict physically realistic values of $\mathbf{S}$ and λ. Furthermore, an additional implication is that the primary problem with the various versions of the tube model lies in the respective evolution equations for $\mathbf{S}$ and λ; therefore, any possible incorporation of the chain-tumbling phenomenon should also include changes to the evolution equation of the orientation tensor, not only the equation for the tube stretch as proposed by Costanzo *et al.* [12].

In light of the above remarks, it is worthwhile to examine whether or not the above statements are also applicable to a transient shear flow situation. In Fig. 7 the transient shear viscosity η^+ is plotted versus time as obtained directly from the NEMD simulations at Wi = 1000 (the dark blue curve). These data exhibit an initial overshoot followed by a small undershoot at longer times, in agreement with typical experimental data for this rheological characteristic function. Plotted alongside these data are the predictions of the DEMG (red curve) and DEMGR (purple curve) tube models. Both models predict an overshoot in the transient viscosity that is significantly higher and shifted to longer times as compared to the NEMD data; however, neither model predicts a subsequent undershoot and eventual damping to a steady-state value. As already noted above, the rotation-enabled DEMGR model possesses a steady-state value of viscosity that is significantly lower than that of the basic DEMG model (and is equivalent to the steady-state value of the original DE model). These data suggest that neither model, or any of the other ones considered in this article, is fully capable of describing actual transient viscosity data at this high Wi. This is congruent with our conclusions from examining the steady-state system properties, as described above.

Also plotted in Fig. 7 are data obtained from using S^t_{xy} as computed using the NEMD simulations with the tube stretch calculated according to Eq. (2) with $\varphi = 1$ (labeled λ_{DEMG}) and subsequently inserted into Eq. (14) to calculate the viscosity; these data are displayed by the black curve. Although the steady-state data of Fig. 3 suggested that Eq. (2) with $\varphi = 1$ might be adequate for calculating the tube stretch variable in steady shear flow, the transient data suggest otherwise. Indeed, the magnitude and position of the overshoot are shifted to higher values of viscosity and time, respectively, although

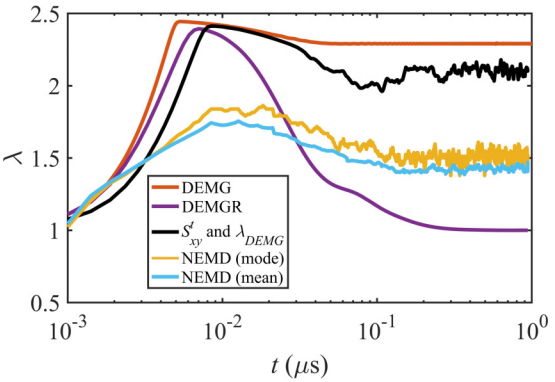

FIG. 8. Transient tube stretch values at Wi = 1000 upon startup of shear flow vs time. The light blue and yellow curves correspond to $\lambda^{\text{mean}}_{\text{NEMD}}$ and $\lambda^{\text{mode}}_{\text{NEMD}}$, respectively, as obtained directly from the simulation data. The red and purple curves are the predictions for tube stretch from the DEMG and DEMGR models, respectively, and the black curve is the prediction for tube stretch arising from Eq. (2) with $\varphi = 1$ once S^t_{xy} has been computed from the NEMD simulations.

the undershoot exhibited by the NEMD data appears to have been predicted by the model albeit shifted to longer times. In some respects, however, the transient predictions of the DEMG model are slightly better than those obtained using S^t_{xy} and λ_{DEMG}, in contrast to the steady-state data; i.e., although the peak value of the DEMG model is higher relative to the NEMD data than that obtained via S^t_{xy} and λ_{DEMG}, the peak position of the DEMG model is closer to the actual peak of the NEMD data.

The light blue and yellow curves in Fig. 7 display data that were calculated using S^t_{xy} from the NEMD simulations, but rather than calculating λ_{DEMG} via Eq. (2), this quantity was computed directly from the simulations using the Z1 code [24] to calculate instantaneous ensemble probability distribution functions (such as displayed in Fig. 4) and then smoothed out using a running time average over ten successive sample times. Both mean and mode methods were used to determine $\lambda^{\text{mean}}_{\text{NEMD}}$ and $\lambda^{\text{mode}}_{\text{NEMD}}$ as functions of time. The results are consistent with each other and indicate that when both S^t_{xy} and either $\lambda^{\text{mean}}_{\text{NEMD}}$ or $\lambda^{\text{mode}}_{\text{NEMD}}$ are calculated directly from the simulation data, the stress expression of Eq. (14) predicts very well the properties of the transient viscosity, namely, the overshoot peak position and height and the approximate location of the undershoot.

To investigate deeper into the fundamental physics underlying the results presented in Fig. 7, the tube stretch is plotted versus time in Fig. 8 at Wi = 1000 under various circumstances. The light blue and yellow curves are data determined directly from the NEMD simulations using the mean and mode methods: $\lambda^{\text{mean}}_{\text{NEMD}}$ or $\lambda^{\text{mode}}_{\text{NEMD}}$. Upon startup of shear, these quantities behave similarly: Each experiences an overshoot followed by a long-time decay to a steady-state plateau. As discussed above, the mode method produces a steady-state value of tube stretch that is slightly higher than that of the mean method. Interestingly, the peak position of the tube stretch is quite different from the corresponding peak position of the viscosity, shown in Fig. 7, which seems to indicate that the overshoot in viscosity is not a direct by-product of the tube stretching mechanism. The purple curve in Fig. 8 corresponds to the prediction of λ of the DEMGR model, which decays to a steady-state value of unity, as explained above. The DEMG model prediction ultimately decays to a steady-state value that is significantly higher than the actual NEMD value, either mean or mode, also as described above. The most interesting feature to note from Fig. 8, however, is the fact that black curve, corresponding to calculating first S^t_{xy} and then using Eq. (2) with $\varphi = 1$ to determine λ_{DEMG} is a surprisingly poor representation of the actual NEMD tube stretch. Hence, in transient situations, there is little evidence to support the fundamental physical mechanisms prescribed by either the DEMG or DEMGR set of evolution equations at high shear rates.

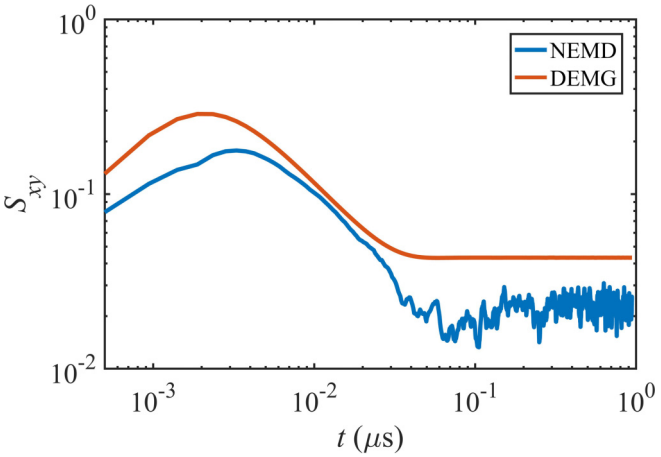

FIG. 9. Tube orientation tensor component S_{xy} at Wi = 1000 upon startup of shear flow vs time. The blue curve corresponds to data computed directly from the NEMD simulations. The red curve is the predictions for S_{xy} of the DEMG and DEMGR models, which are equivalent for all flows.

The tube orientation tensor component S^t_{xy} is plotted versus time at Wi = 1000 as computed directly from the NEMD simulations (blue curve) and as predicted by the DEMG and DEMGR models (red curve), which are equivalent in this case because both models use Eq. (1) to describe the evolution in time of S^t_{xy}. The simulation data show both an overshoot and undershoot with respect to time, but in this case, the tube models overpredict both the transient and steady-state values of S^t_{xy} and greatly underestimate the peak position of the overshoot. Furthermore, neither model displays the undershoot, which is critical to describing the corresponding feature of the transient startup viscosity curve of Fig. 7. Further insight can be gleaned by comparing the positions of the overshoot and undershoot positions in the NEMD data curves of viscosity, tube stretch, and orientation, as observed from Figs. 7, 8, and 9, respectively. The overshoot of the viscosity data in Fig. 7 peaks at 0.004 μs and the undershoot attains its nadir at 0.07 μs. The corresponding values of the tube stretch are 0.01 and 0.16 μs, respectively, and those of the orientation tensor component S^t_{xy} are 0.003 and 0.07 μs. Note that the overshoot and undershoot of the viscosity match fairly well with the corresponding features of the tube orientation tensor, but not very well with those of the tube stretch. Hence it appears that there is a definite lag time between the orientation of the tubes and the subsequent tube stretching and that the transient features of the viscosity are more tuned to the former than the latter. This is an important point to be considered when developing more physically accurate evolution equations for further possible refinement of tube models.

In light of the above observations and remarks, it is necessary to examine carefully the fundamental physical foundation of the tube model under high-Wi flow. In particular, since both $\mathbf{S}$ and λ seem to be poorly described by the underlying theory, one must ponder what other critical features of general tube theory must also be called into question and scrutinized. One of the key lessons learned from the simulations of Nafar Sefiddashti *et al.* [14,15] is that the number of chain entanglements sharply declines at high Wi, thus enabling the individual chain rotation and retraction cycles that lead to the unorthodox features observed in both prior experimental and simulation studies. As many past research works have shown, the flow-induced changes in λ are a critical piece of the puzzle that must be described successfully in order to describe correctly the essential physics of the flow problem; however, other key variables, such as the entanglement number and Rouse time, are generally assumed to remain constant at their equilibrium values, which is not necessarily the case.

In Fig. 10, the top graph shows the number of kinks per chain $\langle Z_k \rangle$ as calculated according to the Z1 code [24] vs tube stretch. At equilibrium, $\langle Z_k \rangle$ is typically twice the number of chain

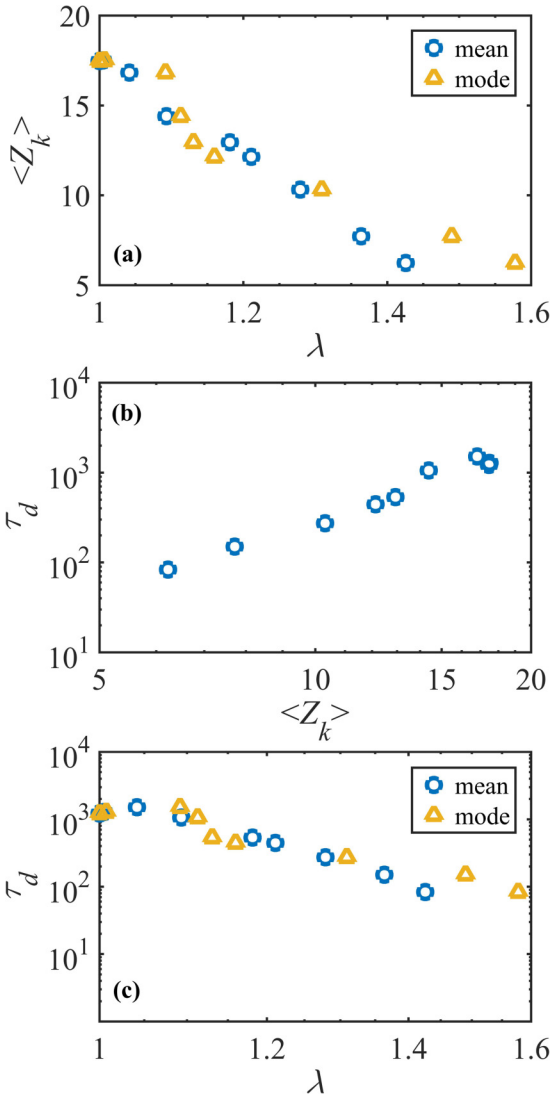

FIG. 10. Number of chain kinks $\langle Z_k \rangle$ plotted as a function of $\lambda_{\text{NEMD}}^{\text{mean}}$ and $\lambda_{\text{NEMD}}^{\text{mode}}$, respectively (top graph), disengagement time plotted vs number of chain kinks (middle graph), and disengagement time plotted vs tube stretch (bottom graph).

entanglements. As shown in the figure, the kink number declines in an almost linear fashion with the increase in the degree of tube stretch induced by the shear flow. This provides direct evidence that there is a direct correlation between the length of the reptation tubes and the entanglements of the surrounding chain network. The middle plot displays the correlation between the disengagement time and the entanglement density of the liquid. The disengagement time was calculated based on the longest relaxation time of the autocorrelation function of the unit end-to-end vectors of the simulated polyethylene chain liquid (see Refs. [14,15] for more details). This plot reveals that the disengagement time decreases in a power-law fashion with respect to the kink number [15]; this translates to the bottom plot, which shows a similar behavior of the disengagement time with respect to the tube stretch variable. The power-law exponent of the curve fitting in Fig. 10(b) is 2.8, which is fairly close to the theoretical scaling of 3 under quiescent conditions.

Clearly, as the tubes stretch and the entanglement number declines, the chains are less confined and restricted translationally, allowing them to diffuse from their initial tubes at greater rates. Nevertheless, the physical relationships and mechanisms governing these altered dynamical states are yet to be incorporated into contemporary tube theory.

IV. CONCLUSION

Viewed as virtual experiments, the results of a recent NEMD simulation study of a moderately entangled polyethylene $C_{700}H_{1402}$ liquid were compared with several versions of the tube model, including a rotation-enabled model that had been recently proposed by Costanzo *et al.* [12] to incorporate the dynamical mechanism of individual chain rotation at high Wi. All of the models examined revealed stark departures from the simulation data under both steady and transient shear flows at high Wi. By examining the key theoretical variables, the tube orientation tensor and the tube stretch, it was shown that although usage of these variables to quantify the corresponding physical property appeared to be physically reasonable, the evolution equations for these variables arising from the various tube models were not appropriate for describing the dynamics of the actual flow process. Possible reasons for this include the averaging procedure used to reduce the stochastic Fokker-Planck equation to a continuum set of equations in terms of preaveraged bulk properties and the possibility of missing physics in such key conceptual quantities as the number of entanglements and disengagement time. Another key finding was that the overshoot and undershoot commonly observed at high shear rate for entangled polymeric liquids can most likely be solely attributed to tube orientation rather than tube stretching. Future theoretical efforts should focus not only on addressing the issues involving the evolution equations for $\mathbf{S}$ and λ, but also on the nature of other dynamical quantities, such as $\langle Z_k \rangle$ and τ_d, at high Wi.

ACKNOWLEDGMENTS

Computational resources were provided by the National Science Foundation under Grant No. CBET-0742679 to the PolyHub Engineering Virtual Organization (EVO) as well as allocation of advanced computational resources on DARTER by the National Institute for Computational Sciences. Financial support was also provided by the National Science Foundation under Grant No. CBET-1602890. All data generated within the scope of this work are freely available to members of the PolyHub EVO.

[1] P. G. de Gennes, Reptation of a polymer chain in the presence of fixed obstacles, J. Chem. Phys. **55**, 572 (1971).
[2] M. Doi and S. F. Edwards, *The Theory of Polymer Dynamics* (Oxford University Press, New York, 1986).
[3] J. M. Dealy and R. G. Larson, *Structure and Rheology of Molten Polymers* (Hanser, Munich, 2006).
[4] G. Marrucci and N. Grizzuti, Fast flows of concentrated polymers-predictions of the tube model on chain stretching, Gazz. Chim. Ital. **118**, 179 (1988).
[5] D. W. Mead, R. G. Larson, and M. Doi, A molecular theory for fast flows of entangled polymers, Macromolecules **31**, 7895 (1998).
[6] G. Marrucci, Dynamics of entanglements: A nonlinear model consistent with the Cox-Merz rule, J. Non-Newtonian Fluid Mech. **62**, 279 (1996).
[7] G. Ianniruberto and G. Marrucci, On compatibility of the Cox-Merz rule with the model of Doi and Edwards, J. Non-Newtonian Fluid Mech. **65**, 241 (1996).
[8] G. Ianniruberto and G. Marrucci, A simple constitutive equation for entangled polymers with chain stretch, J. Rheol. **45**, 1305 (2001).

[9] A. E. Likhtman and R. S. Graham, Simple constitutive equation for linear polymer melts derived from molecular theory: Rolie-Poly equation, J. Non-Newtonian Fluid Mech. **114**, 1 (2003).
[10] R. S. Graham, A. E. Likhtman, T. C. B. McLeish, and S. T. Milner, Microscopic theory of linear, entangled polymer chains under rapid deformation including chain stretch and convective constraint release, J. Rheol. **47**, 1171 (2003).
[11] J. Fang, M. Kröger, and H. C. Öttinger, A thermodynamically admissible reptation model for fast flows of entangled polymers. II. Model predictions for shear and extensional flows, J. Rheol. **44**, 1293 (2000).
[12] S. Costanzo, Q. Huang, G. Ianniruberto, G. Marrucci, O. Hassager, and D. Vlassopoulos, Shear and extensional rheology of polystyrene melts and solutions with the same number of entanglements, Macromolecules **49**, 3925 (2016).
[13] J. M. Kim, B. J. Edwards, D. J. Keffer, and B. Khomami, Dynamics of individual molecules of linear polyethylene liquids under shear: Atomistic simulation and comparison with a free-draining bead-rod chain, J. Rheol. **54**, 283 (2010).
[14] M. H. Nafar Sefiddashti, B. J. Edwards, and B. Khomami, Individual chain dynamics of a polyethylene melt undergoing steady shear flow, J. Rheol. **59**, 119 (2015).
[15] M. H. Nafar Sefiddashti, B. J. Edwards, and B. Khomami, Steady shearing flow of a moderately entangled polyethylene liquid, J. Rheol. **60**, 1227 (2016).
[16] J. M. Kim, B. J. Edwards, D. J. Keffer, and B. Khomami, Single-chain dynamics of linear polyethylene liquids under shear flow, Phys. Lett. A **373**, 769 (2009).
[17] J. M. Kim, B. J. Edwards, and D. J. Keffer, Visualization of conformational changes of linear short-chain polyethylenes under shear and elongational flows, J. Mol. Graphics Model. **26**, 1046 (2008).
[18] J. M. Kim, D. J. Keffer, M. Kröger, and B. J. Edwards, Rheological and entanglement characteristics of linear-chain polyethylene liquids in planar Couette and planar elongational flows, J. Non-Newtonian Fluid Mech. **152**, 168 (2008).
[19] P. S. Stephanou, T. Schweizer, and M. Kröger, Appearance of undershoots in start-up shear: Experimental findings captured by tumbling-snake dynamics, J. Chem. Phys. **146**, 161101 (2017).
[20] C. F. Curtiss and R. B. Bird, A kinetic theory for polymer melts. I. The equation for the single-link orientational distribution function, J. Chem. Phys. **74**, 2016 (1981).
[21] P. S. Desai and R. G. Larson, Constitutive model that shows extension thickening for entangled solutions and extension thinning for melts, J. Rheol. **58**, 255 (2014).
[22] D. S. Pearson, A. D. Kiss, L. J. Fetters, and M. Doi, Flow-induced birefringence of concentrated polyisoprene solutions, J. Rheol. **33**, 517 (1989).
[23] G. Marrucci, F. Greco, and G. Ianniruberto, Integral and differential constitutive equations for entangled polymers with simple versions of CCR and force balance on entanglements, Rheol. Acta **40**, 98 (2001).
[24] M. Kröger, Shortest multiple disconnected path for the analysis of entanglements in two-and three-dimensional polymeric systems, Comput. Phys. Commun. **168**, 209 (2005).